

# An a posteriori verification method for generalized Hermitian eigenvalue problems in large-scale electronic state calculations

Takeo Hoshi<sup>a</sup>, Takeshi Ogita<sup>b</sup>, Katsuhisa Ozaki<sup>c</sup>, Takeshi Terao<sup>d</sup>

<sup>a</sup>Department of Applied Mathematics and Physics, Tottori University, Japan

<sup>b</sup>Division of Mathematical Sciences, Tokyo Woman's Christian University, Japan

<sup>c</sup>Department of Mathematical Sciences, Shibaura Institute of Technology, Japan

<sup>d</sup>Graduate School of Engineering and Science, Shibaura Institute of Technology, Japan

---

## Abstract

An a posteriori verification method is proposed for the generalized Hermitian eigenvalue problems that appear in large-scale electronic state calculations. The method is realized by the two stage process in which the approximate solution is generated by existing numerical libraries and then is verified with a moderate computational time. The procedure indicates that one of exact eigenvalue is located in an interval. Test calculations were carried out for organic device materials and the verification method confirms that all the exact eigenvalues are well separated in the obtained intervals. The verification method will be integrated into EigenKernel (<https://github.com/eigenkernel/>), a middleware for the various parallel solvers in the generalized eigenvalue problem. Such an a posteriori verification method will be important in the future computational science.

(c) 2005 Elsevier B.V. All rights reserved.

**Keywords:** verification method, generalized Hermitian eigenvalue problem, electronic state calculation, supercomputer,  
 2000 MSC: 65F15, 65G20

---

## 1. Introduction

A crucial issue of verification methods is the application to large-scale scientific or industrial computations on supercomputer. The present paper focuses on the generalized Hermitian eigenvalue problem

$$Ax_k = \lambda_k Bx_k \quad (1)$$

under the generalized orthogonality condition

$$x_i^H Bx_j = \begin{cases} 1 & \text{if } i = j \\ 0 & \text{otherwise} \end{cases}, \quad (2)$$

where both  $A$  and  $B$  are Hermitian  $n \times n$  matrices with  $B$  being positive definite. Here we assume that

$$\lambda_1 \leq \lambda_2 \leq \dots \leq \lambda_n.$$

The present problem is motivated by large-scale electronic state calculation, one of the major fields in computational material science and engineering.

This paper proposes an a posteriori verification method for (1), whose workflow is illustrated in Fig. 1; First, an approximate solution is obtained and then is verified. The former and the latter procedures are called solver and verifier, respectively. Our goal is to integrate the verifier routine, as an optional function, to existing numerical solver libraries. One of the author (T. H.) developed a middleware EigenKernel [8, 16, 28] with various parallel solvers for generalized eigenvalue problems and plans to add the functionality of the verifier routine. The total elapsed time  $T_{\text{tot}}$  is the sum of the times for the solver  $T_{\text{sol}}$  and the verifier  $T_{\text{veri}}$  ( $T_{\text{tot}} = T_{\text{sol}} + T_{\text{veri}}$ ). We aim to construct the verifier

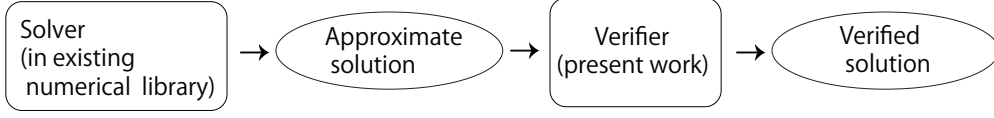


Figure 1: Schematic figure of the workflow with a posteriori verification method.

algorithm so that the time for verifier gives a moderate fraction with  $T_{\text{veri}}$  being comparable to  $T_{\text{sol}}$ . An important feature of a priori verification methods is that the verifier can be independent of the solver, and can use the highly optimized routines of matrix multiplication. Therefore, a priori verification methods are suitable for high-performance computing.

In the solver procedure, approximate solutions  $(\hat{\lambda}_k, \hat{x}_k)$ ,  $k = 1, 2, \dots, n$ , such that

$$A\hat{x}_k \approx \hat{\lambda}_k B\hat{x}_k \quad (3)$$

are obtained by any numerical solver algorithm. The verifier procedure gives mathematical relations, as the difference between the exact and approximate solutions, such as  $|\lambda_k - \hat{\lambda}_k|$  or  $\|x_k - \hat{x}_k\|$ . If one obtains a relation  $|\lambda_k - \hat{\lambda}_k| \leq r_k$  with a given positive number  $r_k$ , for example, it indicates that the exact solution  $(\lambda_k)$  lies in the disk of which center or radius is  $\hat{\lambda}_k$  or  $r_k$ , respectively.

The a posteriori verification strategy is important mainly in three aspects; First, large-scale matrix problems have the potential difficulty for reliable numerical solutions. Among several problems, for example, the difference of sequential eigenvalues ( $\delta_i \equiv \lambda_{i+1} - \lambda_i$ ,  $1 \leq i \leq n - 1$ ) tends to be proportional to  $1/n$  ( $\delta_i \propto 1/n$ ). Consequently many eigenvalues are almost degenerated ( $\delta_i \rightarrow 0$ ) in a large-matrix problem ( $n \rightarrow \infty$ ) and it may be difficult to distinguish them numerically. Second, various numerical algorithms are now proposed for efficient parallel computations, so as to be suitable to current and next-generation supercomputers. Application researchers would like to compare them, both in the computational time and the numerical reliability. Third, the emergence of machine learning enhances to design computer architecture so as to accelerate low precision (single or half) calculation. The efficient use of low precision calculation, typically in a mixed precision calculation, will be important in any high-performance computational science field [6, 1]. A posteriori verification methods will be crucial, so as to guarantee the satisfactory numerical reliability with the use of low precision calculation.

The present paper is organized as follows; Section 2 explains the physical and mathematical backgrounds. The proposed verification method and its numerical examples are appear in Sec. 3 and Sec. 4, respectively. Section 5 gives summary and future aspect.

## 2. Background

### 2.1. Generalized Hermitian eigenvalue problems in electronic state calculations

This section introduces a generalized eigenvalue problem as a numerical foundation of large-scale electronic state calculations. Details can be found in textbooks, such as Ref. [20]. The fundamental Schrödinger-type equation, a linear partial differential equation, is written for an electronic wave function  $\phi(\mathbf{r})$  in real space for a position vector  $\mathbf{r} = (x, y, z)$  as

$$H\phi(\mathbf{r}) = \lambda\phi(\mathbf{r}) \quad (4)$$

with the Hamilton operator

$$H \equiv -\frac{\hbar^2}{2m}\Delta + V_{\text{eff}}(\mathbf{r}). \quad (5)$$

Here,  $\Delta = \partial_x^2 + \partial_y^2 + \partial_z^2$  is Laplacian,  $m$  is the mass of electron,  $\hbar$  is the Planck constant, a physical constant ( $\hbar \approx 1.05 \cdot 10^{-34}$  Js), and  $V_{\text{eff}}(\mathbf{r})$  is the effective potential, a scalar function. The normalization condition

$$\int |\phi(\mathbf{r})|^2 = 1 \quad (6)$$

is imposed and stems from the fact that the sum of the weight distribution of one electron should be the unity.

An eigenvalue  $\lambda$  means the energy of an electron in the material and is called eigenenergy. The  $k$ -th eigenpair  $(\lambda_k, \phi_k(\mathbf{r}))$  is defined for  $k = 1, 2, \dots, n$  in the order of  $\lambda_1 \leq \lambda_2 \leq \dots \leq \lambda_n$ .

Now we consider, as a typical case, that  $\phi(\mathbf{r})$  is expressed as a linear combination of given basic functions

$$\phi(\mathbf{r}) = \sum_j^n c_j \chi_j(\mathbf{r}), \quad (7)$$

where the basis functions  $\{\chi_j(\mathbf{r})\}$  are normalized to be

$$\int \chi_j^*(\mathbf{r}) \chi_j(\mathbf{r}) d\mathbf{r} = 1. \quad (8)$$

A typical basis function is called atomic orbital and is localized near the position of an atomic nucleus. Since each basis function belongs to one atom, the basis index  $i$  is equivalent to the composite indices of an atom index  $I$  and an orbital index  $\alpha$  ( $i \equiv (I, \alpha)$ ). The orbital index  $\alpha$  distinguishes the basis functions that belong to the same atom but different in their shape. Usually, the number of basis functions  $n$  are nearly proportional to the number of atoms  $n_{\text{atom}}$  ( $n \propto n_{\text{atom}}$ ).

When (7) is used for (4), the generalized eigenvalue problem of (1) appears with the Hermitian  $n \times n$  matrices of

$$A_{ij} \equiv \int \chi_i^*(\mathbf{r}) H \chi_j(\mathbf{r}) d\mathbf{r} \quad (9)$$

$$B_{ij} \equiv \int \chi_i^*(\mathbf{r}) \chi_j(\mathbf{r}) d\mathbf{r}. \quad (10)$$

The matrix  $B$  is positive definite and satisfies  $B_{jj} = 1$  and  $|B_{ij}| < 1$  ( $i \neq j$ ). Hereafter we consider, as among many researches, that the basis functions are real and the matrices  $A$  and  $B$  are real symmetric. The normalization condition of (6) is reduced to

$$x_k^T B x_k = 1, \quad (11)$$

which is called  $B$ -normalization.

Here the simplest theory of hydrogen molecule ( $\text{H}_2$ ) is demonstrated, as in many textbooks, like Ref. [2]. The atomic nucleus of the first or second hydrogen atom is located at  $\mathbf{r} = \mathbf{R}_1$  or  $\mathbf{R}_2$ , respectively. We consider a given localized function  $f(\mathbf{r})$  of which localization center is located as  $\mathbf{r} = 0$ . Two basis functions  $\chi_1(\mathbf{r})$  and  $\chi_2(\mathbf{r})$  are prepared as

$$\chi_1(\mathbf{r}) \equiv f(\mathbf{r} - \mathbf{R}_1), \quad \chi_2(\mathbf{r}) \equiv f(\mathbf{r} - \mathbf{R}_2). \quad (12)$$

The generalized eigenvalue problem of (1) appears with the  $2 \times 2$  real symmetric matrices of

$$A \equiv \begin{pmatrix} a & -t \\ -t & a \end{pmatrix}, \quad B \equiv \begin{pmatrix} 1 & s \\ s & 1 \end{pmatrix}. \quad (13)$$

Now we consider a typical case in which  $a, t, s$  are positive real numbers and  $s < 1$ . The offdiagonal element of  $t$  or  $s$  is the function of the interatomic distance  $d \equiv |\mathbf{R}_1 - \mathbf{R}_2|$  ( $t = t(d), s = s(d)$ ). The eigenvalues are

$$\lambda_1 \equiv \frac{a-t}{1+s}, \quad \lambda_2 \equiv \frac{a+t}{1-s} \quad (14)$$

and the eigenvectors are

$$x_1 = \frac{1}{\sqrt{2(1+s)}} \begin{pmatrix} 1 \\ 1 \end{pmatrix}, \quad x_2 = \frac{1}{\sqrt{2(1-s)}} \begin{pmatrix} 1 \\ -1 \end{pmatrix}. \quad (15)$$

The matrix  $B$  has the eigenvalues of  $1 \pm s$  and will be not positive definite in the limiting situation of  $s \rightarrow 1$ . Such limiting situation appears when the distance between the atoms nuclei is almost zero ( $d \rightarrow 0$ ) or the two basis functions will be identical ( $\chi_1(\mathbf{r}) - \chi_2(\mathbf{r}) \rightarrow 0$ ).

Matrix data of  $A$  and  $B$  for various materials are stored in ELSSES matrix library [21, 14]. The matrix data were generated by the electronic-state calculation software ELSSES [9, 15, 13] with first-principles-based modeled (tight-binding) electronic-state theory. The atomic unit is used for the energy among the data files. For many problems, the approximate eigenvalues  $\{\hat{\lambda}_k\}$  are uploaded, as well as the matrix data of  $A$  and  $B$ , for researcher's convenience. The sparsity of the stored matrix data of  $A_{ij}$  and  $B_{ij}$  are explained briefly. As explained above, the indices  $i$  and  $j$  are the composite indices of the atom indices  $I$  and  $J$  and the orbital indices  $\alpha$  and  $\beta$ , respectively ( $i \equiv i(I, \alpha)$ ,  $j \equiv j(J, \beta)$ ). Therefore, an element of the matrices  $A$  and  $B$  is expressed by the four indices as  $A_{I\alpha;J\beta}$  and  $B_{I\alpha;J\beta}$ , respectively. Since a matrix element value decreases quickly and monotonically as the function of the inter-atomic distance between the  $I$ -th and  $J$ -th atoms ( $r_{IJ}$ ), a cutoff distance  $r_{\text{cut}}$  can be introduced. A matrix element,  $A_{I\alpha;J\beta}$  or  $B_{I\alpha;J\beta}$ , is ignored, if  $r_{IJ} > r_{\text{cut}}$ , which makes the matrices to be sparse. More information of the data file in ELSSES matrix library is found in Ref. [14].

## 2.2. Numerical solvers for generalized eigenvalue problem

Here an overview is given for the parallel dense-matrix solver of the generalized eigenvalue problem of (1), in particular, for the variety of the used algorithms. The solver algorithm for (1) consists of four procedures; (i) Cholesky decomposition of  $B$ ;

$$B = R^T R, \quad (16)$$

with an upper triangular matrix  $R$ , (ii) reduction to the standard eigenvalue problem (SEP)

$$A' y_k = \lambda_k y_k, \quad (17)$$

with

$$A' \equiv R^{-T} A R^{-1}, \quad (18)$$

(iii) solution of the standard eigenvalue problem (17), and (iv) transformation of the eigenvectors;

$$x_k = R^{-1} y_k. \quad (19)$$

The set of the procedures (i), (ii), and (iv) is called reducer, and the procedure (iii) is called SEP solver.

Although ScaLAPACK [27, 3] is the *de facto* standard parallel numerical library, it was developed mainly in 1990s and several routines show severe bottlenecks on modern massively parallel supercomputers. Novel solver libraries of ELPA [10, 19] and EigenExa [7, 17] were proposed, so as to overcome the bottlenecks. The ELPA code was developed in Europe under the tight collaboration between computer scientists and material science researchers and its main target application is FHI-aims [11, 4], a famous electronic state calculation code. The EigenExa code, on the other hand, was developed at RIKEN in Japan. It is an important fact that the ELPA code has routines optimized for x86, IBM Blue-Gene, and AMD architectures, while the EigenExa code was developed so as to be optimal mainly on the K computer, a Japanese flagship supercomputer. Both ScaLAPACK and ELPA provide the reducer routines, and all of ScaLAPACK, ELPA, and EigenExa provide the SEP solver routines.

Since the computational performance depends both on problem and architecture, it is, in principle, possible to construct a 'hybrid' workflow in which one chooses the reducer routine from one library and the SEP solver routine from another library, so as to realize the optimal performance. The middleware EigenKernel was developed in order to realize the hybrid workflows. An obstacle for realizing the hybrid workflow is the difference of matrix distribution schemes between different libraries. EigenKernel provides the data conversion routines between libraries and surmounts the obstacle. Figure 2 shows the possible workflows for a future version of EigenKernel with the a posteriori verification routine.

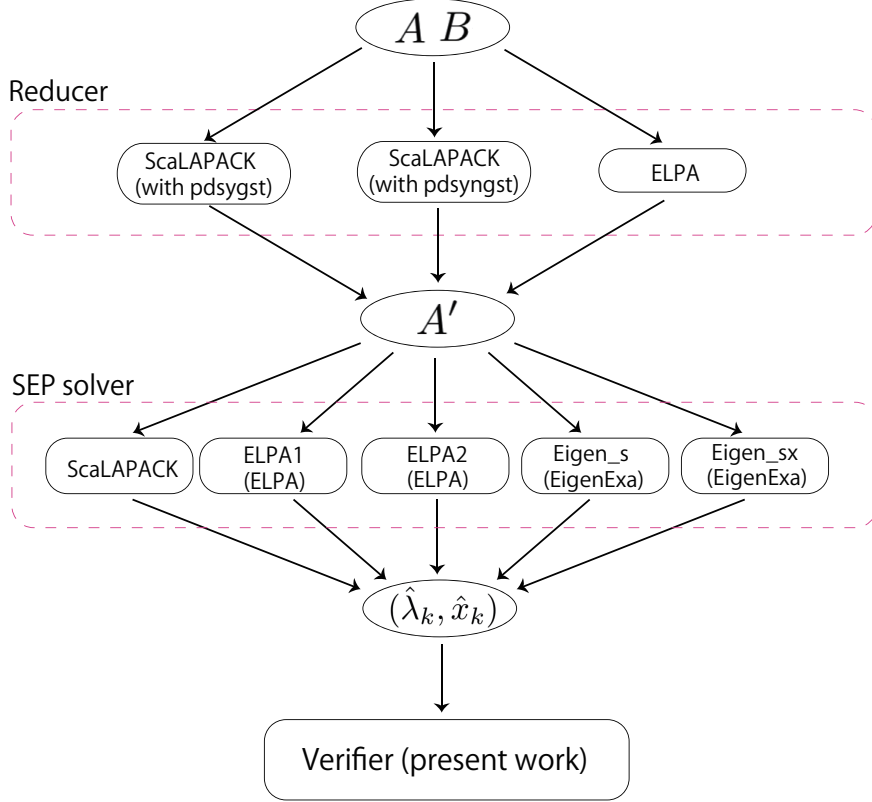


Figure 2: Schematic figure of the possible hybrid workflows for a future version of EigenKernel with the a posteriori verification routine. Two routines in ScaLAPACK and one routine in ELPA are available for the reducer, while one routine in ScaLAPACK and two routines in ELPA and EigenExa are for the SEP solver. The a posteriori verification routine is used commonly among the workflows.

### 2.3. Verified numerical computations

We briefly explain how to obtain mathematically rigorous numerical results using floating-point arithmetic. Let  $\mathbb{F}$  and  $\mathbb{IF}$  be sets of floating-point numbers and intervals, respectively. We use bold-faced letters for interval matrices, whose elements are intervals. For an interval matrix  $\mathbf{C}$ ,  $C_{\text{inf}}$  and  $C_{\text{sup}}$  denote the left and right endpoints, respectively, such that  $\mathbf{C} = [C_{\text{inf}}, C_{\text{sup}}]$ , i.e.,  $\mathbf{C}_{ij} = [(C_{\text{inf}})_{ij}, (C_{\text{sup}})_{ij}]$  for all  $(i, j)$  pairs. In addition,  $C_{\text{mid}}$  and  $C_{\text{rad}}$  denote the midpoint and the radius of  $\mathbf{C}$ , respectively, such that  $\mathbf{C} = [C_{\text{mid}} - C_{\text{rad}}, C_{\text{mid}} + C_{\text{rad}}]$ . Let  $fl(\cdot)$ ,  $fl_{\nabla}(\cdot)$ , and  $fl_{\Delta}(\cdot)$  be computed results by floating-point arithmetic defined in IEEE 754 with rounding to the nearest (roundTiesToEven), rounding downwards (roundTowardNegative), and rounding upwards (roundTowardPositive), respectively.

We review basic interval matrix multiplication in [25]. For two point matrices  $P, Q \in \mathbb{F}^{n \times n}$ , the matrix product  $PQ \in \mathbb{R}^{n \times n}$  can be enclosed as

$$PQ \in [fl_{\nabla}(PQ), fl_{\Delta}(PQ)], \quad (20)$$

where two matrix multiplications are required. For a point matrix  $P \in \mathbb{F}^{n \times n}$  and an interval matrix  $\mathbf{Q} \in \mathbb{IF}^{n \times n}$ , the product  $P\mathbf{Q}$  can be enclosed as

$$P\mathbf{Q} \subset [fl_{\nabla}(PQ_{\text{mid}} - fl_{\Delta}(|P|Q_{\text{rad}})), fl_{\Delta}(PQ_{\text{mid}} + fl_{\Delta}(|P|Q_{\text{rad}}))]. \quad (21)$$

It involves three matrix multiplications, since  $fl_{\Delta}(|P|Q_{\text{rad}})$  is common for calculating the left and right endpoints. Note that if the interval matrix  $\mathbf{Q}$  is given by the “inf-sup” form  $[Q_{\text{inf}}, Q_{\text{sup}}]$ , we can easily obtain the midpoint  $Q_{\text{mid}}$  and the radius  $Q_{\text{rad}}$  such that  $[Q_{\text{inf}}, Q_{\text{sup}}] \subset [Q_{\text{mid}} - Q_{\text{rad}}, Q_{\text{mid}} + Q_{\text{rad}}]$ . Moreover, for given matrices  $P = (p_{ij}), Q = (q_{ij}) \in \mathbb{F}^{n \times n}$ , the notation  $\max(P, Q)$  means  $\max(p_{ij}, q_{ij})$  for all  $(i, j)$  pairs, i.e., the maximum is taken componentwise.

There exist several implementations of the above interval arithmetic for matrix multiplication, e.g., C-XSC [5], a C++ library and INTLAB [26], a Matlab/Octave toolbox for verified numerical computations. Both C-XSC and INTLAB share the common feature that utilizes BLAS (Basic Linear Algebra Subprograms) routines. In other words, we can efficiently implement interval matrix multiplication using PBLAS, the parallel version of BLAS, on distributed computer environments, as long as directed rounding in floating-point operations is available in BLAS routines for matrix multiplication and the reduction operation of summation.

### 3. A posteriori verification methods

#### 3.1. Possible verification methods

Possible verification methods are discussed here. To measure the accuracy of the computed solution  $(\hat{\lambda}_k, \hat{x}_k)$ , application researchers often compute a norm of the residual vector, such as

$$\frac{\|A\hat{x}_k - \hat{\lambda}_k B\hat{x}_k\|_2}{\|\hat{x}_k\|_2}. \quad (22)$$

Although this quantity usually suffices to check whether the solver works correctly, it does not verify the accuracy of the computed eigenvalue. The following inequality is a known residual bound [23]:

$$\min_{1 \leq j \leq n} |\lambda_j - \hat{\lambda}_k| \leq \sqrt{\|B^{-1}\|_2} \frac{\|A\hat{x}_k - \hat{\lambda}_k B\hat{x}_k\|_2}{\sqrt{\hat{x}_k^T B \hat{x}_k}}. \quad (23)$$

From this bound, we can confirm that some eigenvalue of  $(A, B)$  exists in the neighborhood of  $\hat{\lambda}_k$  satisfying (23). However, we cannot determine whether  $\hat{\lambda}_k$  is an approximation of the  $k$ -th eigenvalue of  $(A, B)$ . To understand the electronic state of the problems correctly, it is crucial to determine the order of eigenvalues [18].

To our knowledge, we have the following two possibilities to determine the order of eigenvalues of symmetric matrices:

- Compute all eigenpairs (eigenvalues and eigenvectors), and verify error bounds of all computed eigenvalues (cf. e.g. [23]).
- Compute an approximation  $\hat{\lambda}_k$  of a target eigenvalue using Sylvester's law of inertia with LDL<sup>T</sup> decomposition [18], and verify that  $\hat{\lambda}_k$  is an approximation of the  $k$ -th eigenvalue with an error bound (cf. e.g. [30]).

In this paper, we adopt the former method from the aspect of simpleness and efficiency of code development on supercomputer.

#### 3.2. Proposed method

We aim to obtain componentwise error bounds for computed eigenvalues  $\hat{\lambda}_k, k = 1, 2, \dots, n$ . Let  $X, D \in \mathbb{R}^{n \times n}$  denote a matrix comprising all generalized eigenvectors of  $(A, B)$  and a diagonal matrix of the corresponding generalized eigenvalues such that

$$X = [x_1, x_2, \dots, x_n], \quad D = \text{diag}(\lambda_1, \lambda_2, \dots, \lambda_n).$$

Let  $I$  denote the  $n \times n$  identity matrix. Then we have

$$\begin{cases} AX = BXD, \\ X^T BX = I. \end{cases}$$

Let  $\hat{X} = [\hat{x}_1, \hat{x}_2, \dots, \hat{x}_n] \in \mathbb{R}^{n \times n}$  and  $\hat{D} = \text{diag}(\hat{\lambda}_1, \hat{\lambda}_2, \dots, \hat{\lambda}_n) \in \mathbb{R}^{n \times n}$  as approximation of  $X$  and  $D$ , respectively. Suppose  $\hat{X}$  is nonsingular. Then

$$A\hat{X} \approx B\hat{X}\hat{D}, \quad \hat{X}^T B \hat{X} \approx I \quad \Rightarrow \quad \hat{X}^{-1} B^{-1} A \hat{X} \approx \hat{D}, \quad (B\hat{X})^{-1} \approx \hat{X}^T.$$

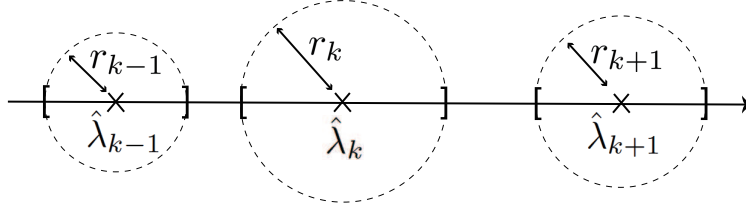


Figure 3: Schematic figure of verified solution, when all the disks are separated and each disk contains precisely one eigenvalue ( $\lambda_k \in [\hat{\lambda}_k - r_k, \hat{\lambda}_k + r_k]$ ).

Since  $\hat{X}^{-1}B^{-1}A\hat{X}$  is a similarity transformation of  $B^{-1}A$ , the eigenvalues of  $\hat{X}^{-1}B^{-1}A\hat{X}$  are the same as those of  $B^{-1}A$  and thus the generalized eigenvalues of  $(A, B)$ .

Here, we aim to compute an inclusion of  $\hat{X}^{-1}B^{-1}A\hat{X}$ . To this end, we here introduce Yamamoto's theorem for verified solutions of linear systems. Note that for a given matrix  $C = (c_{ij}) \in \mathbb{R}^{n \times n}$ , the notation  $|C|$  means  $|C| = (|c_{ij}|) \in \mathbb{R}^{n \times n}$ , and the same applies to vectors, i.e., the absolute value is taken componentwise. For given matrices  $P = (p_{ij}), Q = (q_{ij}) \in \mathbb{R}^{n \times n}$ , the notation  $P \leq Q$  means  $p_{ij} \leq q_{ij}$  for all  $(i, j)$ , and the same applies to vectors, i.e., the inequality holds componentwise. Moreover, define  $e = (1, 1, \dots, 1)^T$ .

**Theorem 1** (Yamamoto [31]). *Let  $A$  and  $C$  be real  $n \times n$  matrices, and let  $b$  and  $\hat{x}$  be real  $n$ -vectors. If  $\|I - CA\|_\infty < 1$ , then  $A$  is nonsingular, and*

$$|A^{-1}b - \hat{x}| \leq |C(b - A\hat{x})| + \frac{\|C(b - A\hat{x})\|_\infty}{1 - \|I - CA\|_\infty} |I - CA|e.$$

We now consider a linear system  $(B\hat{X})Y = A\hat{X}$  for  $Y$  and regard  $\hat{D}$  as its approximate solution. Let  $Y, R$ , and  $G$  be defined as

$$\begin{cases} R \equiv \hat{X}^T(A\hat{X} - B\hat{X}\hat{D}), \\ G \equiv \hat{X}^TB\hat{X} - I. \end{cases}$$

If  $\|G\|_\infty < 1$ , applying Theorem 1 yields

$$|\hat{X}^{-1}B^{-1}A\hat{X} - \hat{D}| \leq |R| + \frac{\|R\|_\infty}{1 - \|G\|_\infty} |G|E \equiv F, \quad (24)$$

where  $E$  is the  $n \times n$  matrix of all 1's.

Let  $\Lambda \equiv \{\lambda_1, \lambda_2, \dots, \lambda_n\}$ . For  $r_i \equiv \sum_{j=1}^n F_{ij}$ , the Gershgorin circle theorem implies

$$\Lambda \subseteq \bigcup_{k=1}^n [\hat{\lambda}_k - r_k, \hat{\lambda}_k + r_k]. \quad (25)$$

If all the disks  $[\hat{\lambda}_i - r_i, \hat{\lambda}_i + r_i]$  are isolated, then all the eigenvalues are separated, i.e., each disk contains precisely one eigenvalue of  $B^{-1}A$  [29, pp. 71ff], as schematically shown in Fig. 3. If several disks are overlapped such that  $|\hat{\lambda}_{k+1} - \hat{\lambda}_k| > r_k + r_{k+1}$ , it indicates that some of the eigenvalues are degenerated or nearly degenerated. Moreover, if  $B$  is ill-conditioned, then the  $B$ -orthogonality of  $\hat{X}$  may break down such that  $\|G\|_\infty \geq 1$ . In such a case, Theorem 1 cannot be applied, and the verification procedure must end in failure. Therefore, we need to check whether  $\|G\|_\infty < 1$  in code development from the verification method.

In [22], a similar method has been proposed. The proposed method can be regarded as a variant of the method in [22] specialized for symmetric eigenvalue problems.

### 3.3. Code development

We explain how to obtain an upper bound of the vector  $r$  in (25) using only floating-point arithmetic. We first focus on how to obtain the upper bound of  $|R| = |\hat{X}^T(A\hat{X} - B\hat{X}\hat{D})|$  and  $|G| = |\hat{X}^TB\hat{X} - I|$  in (24). The upper bound for  $|R|$  is obtained as follows:

1.  $\mathbf{C} \leftarrow A\hat{X}$  % Two matrix multiplications based on (20)
2.  $\mathbf{F} \leftarrow B\hat{X}$  % Two matrix multiplications based on (20)
3.  $\mathbf{F} \leftarrow \mathbf{F}\hat{D}$  % negligible cost because  $\hat{D}$  is a diagonal matrix
4.  $\mathbf{C} \leftarrow \mathbf{C} - \mathbf{F}$  % negligible cost,  $C_{\text{inf}}$  is overwritten by  $\text{fl}_{\nabla}(C_{\text{inf}} - F_{\text{sup}})$ ,  $C_{\text{sup}}$  is overwritten by  $\text{fl}_{\Delta}(C_{\text{sup}} - F_{\text{inf}})$
5.  $\mathbf{C} \leftarrow \hat{X}^T \mathbf{C}$  % Three matrix multiplications based on (21)
6.  $|R| \leq \max(|C_{\text{inf}}|, |C_{\text{sup}}|) \equiv R'$

Note that the notation “ $\leftarrow$ ” means enclosure of the result. Thus, seven matrix multiplications are required for the upper bound of  $|R|$ . The upper bound of  $|G|$  is obtained as follows:

1.  $\mathbf{C} \leftarrow B\hat{X}$  % Two matrix multiplications based on (20)
2.  $\mathbf{F} \leftarrow \hat{X}^T \mathbf{C}$  % Three matrix multiplications based on (21)
3.  $\mathbf{W} \leftarrow \mathbf{F} - I$  % negligible cost,  $W_{\text{inf}} \equiv \text{fl}_{\nabla}(F_{\text{inf}} - I)$ ,  $W_{\text{sup}} \equiv \text{fl}_{\Delta}(F_{\text{sup}} - I)$
4.  $|G| \leq \max(|W_{\text{inf}}|, |W_{\text{sup}}|) \equiv G'$

Five matrix multiplications are required for the upper bound of  $|G|$ . Since the enclosure of  $B\hat{X}$  is common for the upper bounds for  $|R|$  and  $|G|$ , we can save two matrix multiplications. Therefore, totally 10 matrix multiplications are required, so that it involves  $20n^3 + O(n^2)$  floating-point operations.

We compute the upper bounds of  $\|R\|_{\infty}$  and  $\|G\|_{\infty}$  as

$$\|R\|_{\infty} \leq \|R'\|_{\infty} \leq \text{fl}_{\Delta}(\|R'\|_{\infty}) \equiv \alpha_1, \quad \|G\|_{\infty} \leq \|G'\|_{\infty} \leq \text{fl}_{\Delta}(\|G'\|_{\infty}) \equiv \alpha_2.$$

If  $\alpha_2 \geq 1$ , then the verification failed. The upper bound of  $Fe$  is obtained by

$$r = Fe \leq \text{fl}_{\Delta} \left( R'e + \frac{n\alpha_1}{\text{fl}_{\nabla}(1 - \alpha_2)} G'e \right) \equiv r'. \quad (26)$$

The routine `pdsygvx` in ScaLAPACK produces computed eigenvalues  $\hat{\lambda}_i$  with  $\hat{\lambda}_1 \leq \hat{\lambda}_2 \leq \dots \leq \hat{\lambda}_n$ . Therefore, if  $\hat{\lambda}_{i+1} - \hat{\lambda}_i > r'_i + r'_{i+1}$  are satisfied for  $1 \leq i \leq n-1$ , then we can separate all the eigenvalues and determine the order of the eigenvalues correctly.

The test code was developed in C language with the parallel libraries of PBLAS and ScaLAPACK. The solver procedure uses a GEP solver routine (`pdsygvx`) in ScaLAPACK, while the verifier routine uses the matrix multiplication routine (`pdgemm`) in PBLAS.

It should be noted that the verifier procedure is simply based on the matrix multiplication operation, while the solver procedure consists of complicated procedures, such as Cholesky decomposition, tridiagonalization, and so forth. Therefore, the verifier procedure is expected to be moderate in computational time and to be efficient in parallelism, when compared to the solver procedure.

## 4. Numerical example

### 4.1. Problem

Numerical examples are shown in this section. The calculated problems are PPE354, PPE3594, PPE7194, PPE177994, PPE107994, VCNT22500, VCNT225000, NCCS430080 in ELSEES matrix library. The number in the problem name indicates the matrix dimension  $n$ . For example, the system PPE354 contains  $n \times n$  matrices  $A$  and  $B$  with  $n = 354$ . All the matrices  $A$  and  $B$  in these systems are real symmetric. The systems with the letter of 'PPE' are those of organic polymers of poly-(phenylene-ethynylene) (PPE). The left panel of Fig. 4(a) shows the Structural formula of PPE. The right panel of Fig. 4(b) shows a part of the polymer in a disordered structure. The difference of the matrix size stems from the length of the polymer chain. The system of PPE354 is, for example, the polymer with  $n = 10$  monomers and  $N_{\text{atom}} = 12n = 120$  atoms. The system VCNT225000 is that of vibrating carbon nanotube (VCNT). The system NCCS430080 is that of nano-composite carbon solid (NCCS) [12]. The matrices are those with disordered atomic structures. Disordered systems are important for industrial application, since most industrial materials are disordered, unlike ideal crystal or periodic structure. Consequently, the eigenvalues are not degenerated among the problems.

The characteristic of the eigenvalue distribution can be captured by the following two quantities; One is the difference of sequential approximate eigenvalues  $\hat{\delta}_k \equiv \hat{\lambda}_{k+1} - \hat{\lambda}_k (k = 1, 2, \dots, n - 1)$ . The other is the eigenvalue count  $I(\lambda)$  that is defined, on the eigenvalue axis  $\lambda$ , as

$$I(\lambda) \equiv \sum_k^n \theta(\lambda_k - \lambda) \quad (27)$$

with the step function

$$\theta(\lambda) \equiv \begin{cases} 1 & (\lambda \geq 0) \\ 0 & (\lambda < 0) \end{cases} \quad (28)$$

In other words, the eigenvalue count  $I(\lambda)$  is the number of the eigenvalues smaller than  $\lambda$ .

Here, we demonstrate of the similarity and the size dependence of eigenvalue distribution among the organic polymer systems. The organic polymers of PPE354, PPE177994 and PPE107994 are picked out. Figure 4(b)(c) shows the normalized eigenvalue distribution  $I(\lambda)/n$  among these three systems. The three polymers give quite similar curves in Fig. 4(b)(c) and therefore the difference  $\hat{\delta}_k$  is nearly proportional to  $1/n$  ( $\hat{\delta}_k \propto 1/n$ ), as explained in Sec. 1.

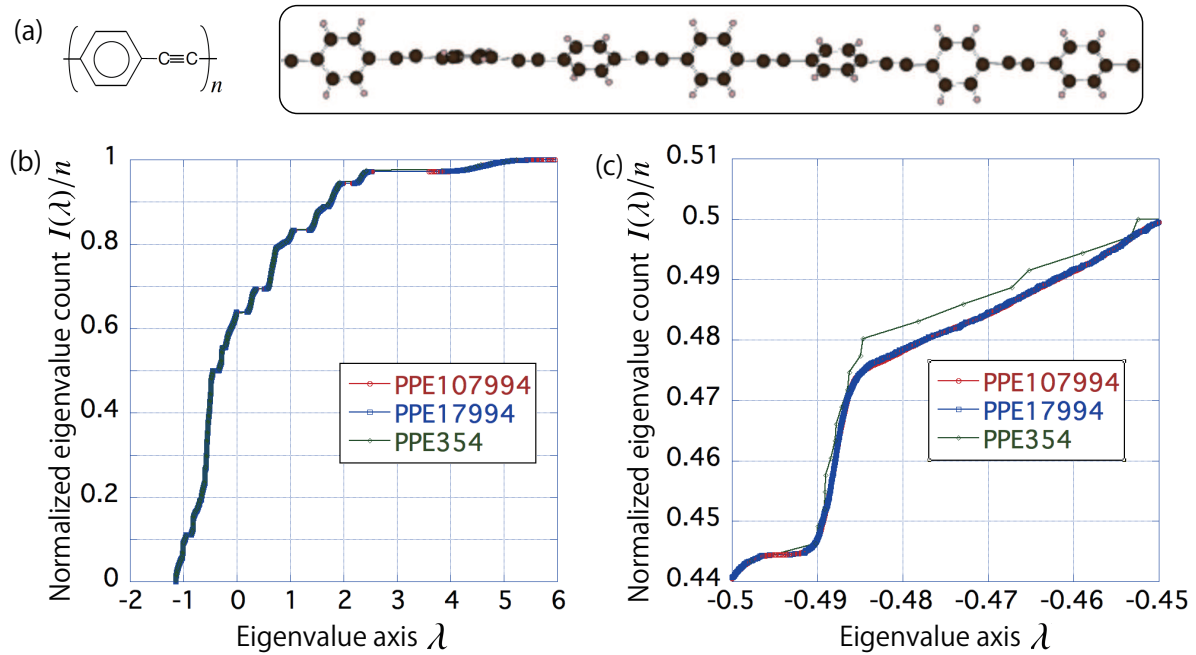


Figure 4: (a) Structural formula (left) and a part of the atomic structure (right) of poly-(phenylene-ethynylene) (PPE). (b) Similarity of eigenvalue distribution in PPE354 (circle), PPE17994 (square) and PPE107994 (diamond). The normalized eigenvalue counts  $I(\lambda)/n$  are plotted on the eigenvalue axis  $\lambda$ . (c) A close-up of (b).

#### 4.2. Result

Tables 1 and 2 show the calculation results on the K computer. First, we focus on numerical results for the approximate eigenvalues  $\hat{\lambda}$  and its upper bound  $r'$ . The routine `pdsygvx` in ScaLAPACK produces  $\hat{\lambda}_1 \leq \hat{\lambda}_2 \leq \dots \leq \hat{\lambda}_n$ . The vector  $r'$  is obtained by (26). Here we define the radius sum  $\rho_k \equiv r'_{k+1} + r'_k$  for  $1 \leq k \leq n - 1$ . We find  $m$  such that  $\hat{\delta}_m - \rho_m = \min_{1 \leq k \leq n-1} (\hat{\delta}_k - \rho_k)$ . The items “Difference” and “Radius” in Table 1 show  $\hat{\delta}_m$  and  $\rho_m$ , respectively. As can be seen,  $\hat{\delta}_m > \rho_m$  is satisfied in all the problems, or all the disks of  $|\lambda_k - \hat{\lambda}_k| < r'_k$  are separated as in Fig. 3. Thus, we can determine the order of eigenvalues in each problem. If  $\hat{\delta}_k < \rho_k$  is satisfied for a  $k$ , the two disks of  $|\lambda_k - \hat{\lambda}_k| < r'_k$  and  $|\lambda_{k+1} - \hat{\lambda}_{k+1}| < r'_{k+1}$  are overlapped and the two exact eigenvalues of  $\lambda_k$  and  $\lambda_{k+1}$  can be degenerated.

Figure 5(a) shows the eigenvalue difference  $\{\hat{\delta}_k\}$  and the radius sum  $\{\rho_k\}$  as the function of the eigenvalue  $\{\hat{\lambda}_k\}$  in the case of PPE107994. One can find that the radius sum satisfies  $\rho_k \leq 10^{-10}$  and is much smaller than the difference ( $\rho_k \ll \hat{\delta}_k$ ), except several points. We found that  $m = 49201$  and  $\hat{\lambda}_{49201} \approx -0.488$ ,  $\hat{\delta}_{49201} \approx 6.42 \times 10^{-11}$ ,  $\rho_{49201} \approx 9.17 \times 10^{-12}$ . Figure 5(b) shows a close-up of Fig. 5(a) and contains the eigenvalue of  $\hat{\lambda}_{49201} \approx -0.488$ . It is reasonable that the eigenvalue  $\hat{\lambda}_{49201}$  appears in the region of  $-0.490 < \lambda < -0.485$ , since many eigenvalues are densely populated and the eigenvalue count  $I(\lambda)$  increases rapidly in the region, as shown in Fig. 4(c). The same analysis was also carried out in the case of NCCS430080, the largest problem among the present calculations, and is shown in Figs 5(c) and (d). One can find that the radius sum satisfies is much smaller than the difference ( $\rho_k \ll \hat{\delta}_k$ ), except several points.

Table 1: Numerical example

Problem name	Matrix dimension ( $n$ )	Difference ( $\hat{\delta}_m$ )	Radius sum ( $\rho_m$ )
PPE354	354	$6.61 \times 10^{-5}$	$4.90 \times 10^{-13}$
PPE3594	3,594	$1.03 \times 10^{-7}$	$1.33 \times 10^{-12}$
PPE7194	7,194	$5.55 \times 10^{-8}$	$1.18 \times 10^{-12}$
PPE17994	17,994	$5.32 \times 10^{-11}$	$2.56 \times 10^{-12}$
PPE107994	107,994	$6.42 \times 10^{-11}$	$9.17 \times 10^{-12}$
VCNT22500	22,500	$2.59 \times 10^{-7}$	$3.20 \times 10^{-10}$
VCNT225000	225,000	$1.97 \times 10^{-9}$	$1.64 \times 10^{-9}$
NCCS430080	430,080	$5.10 \times 10^{-9}$	$1.61 \times 10^{-9}$

Table 2 shows the computational times. The item  $T_{\text{sol}}$  in Table 2 shows the computing time for `pdsygvx` in ScaLAPACK. The item  $T_{\text{veri}}$  shows the computing time for verification process, mainly, the time for matrix multiplications. Here, the verifier consumes a moderate cost ( $T_{\text{veri}} \leq T_{\text{sol}}$ ), as expected in Sec. 3.3. More intensive benchmarks including weak scaling will be carried out in future.

Table 2: Elapsed times among the problems. The number of used processor nodes  $P$ , the elapsed times for the solver  $T_{\text{sol}}$  and verifier  $T_{\text{veri}}$  are shown.

Problem name	$P$	$T_{\text{sol}}$	$T_{\text{veri}}$
PPE354	4	0.32	0.12
PPE3594	4	20.74	4.73
PPE7194	4	118.84	31.74
PPE17994	16	217.91	105.75
PPE107994	600	1009.85	682.92
VCNT22500	64	105.75	59.06
VCNT225000	2025	2625.76	1775.09
NCCS430080	6400	8960.03	3496.56

In conclusion, the verification procedure informs us the intervals that contains the exact eigenvalues ( $|\lambda_k - \hat{\lambda}_k| < r'_k$ ) with the approximate eigenvalues  $\hat{\lambda}_k$  and the radius  $r'_k$ . We will plan to upload the radius data files in ELSSES matrix library, as well as the input matrix data and the approximate eigenvalue data. Then one can draw a graph like one in Fig. 5, so as to measure the accuracy of the computed solutions.

## 5. Summary and future aspect

The present paper proposes an a posteriori verification methods in the generalized eigenvalue problems that appear in large-scale electronic state calculations. The verification procedure gives rigorous mathematical foundation of numerical reliability. Since the verifier procedure consists of simple matrix multiplications, the computational cost is moderate, when compared with that of the solver procedure. Therefore, application researchers can use the verification

function only with a moderate increase of the computational cost. Test calculations were carried out on the K computer for real problems with up to the matrix size of  $n \approx 4 \times 10^5$ .

The next stage of the research is the integration of the present verifier routine and the solver routines by EigenKernel, in which we can use various solver routines among ScaLAPACK and newer libraries and can compare their approximate solutions in the verification procedure.

A future issue is to realize the refinement of approximate solutions, before and/or after the verification procedure. The refinement procedure will be crucial, in particular, when lower precision arithmetic, such as half precision and single precision, is used for calculating an approximate solution as an initial guess. For example, a refinement algorithm for the symmetric eigenvalue problem was recently proposed in [24], which is based on matrix multiplication. Such refinement algorithms enhances application researchers to use lower precision arithmetic with satisfactory reliability of computed results, which will be of great important in next-generation architecture that is optimized for lower precision arithmetic.

## Acknowledgement

The present research was partially supported by MEXT as “Exploratory Issue on Post-K computer” (Development of verified numerical computations and super high-performance computing environment for extreme researches) using computational resources of the K computer provided by the RIKEN R-CCS through the HPCI System Research project (Project ID: hp180222) and Priority Issue 7 of the post-K project. The present research was partially supported by KAKENHI funds (16KT0016,17H02828).

## References

- [1] A. Alvermann, A. Basermann, H.-J. Bungartz, C. Carbogno, D. Ernst, H. Fehske, Y. Futamura, M. Galgon, G. Hager, S. Huber, T. Hucke, Ida, A. Imakura, M. Kawai, S. Köcher, M. Kreutzer, P. Kus, B. Lang, H. Lederer, V. Manin, A. Marek, K. Nakajima, L. Nemeč, K. Reuter, M. Rippl, M. Rhrig-Zöllner, T. Sakurai, M. Scheffler, C. Scheurer, F. Shahzad, D. S. Brambila, J. Thies, and G. Wellein. Benefits from using mixed precision computations in the ELPA-AEO and ESSEX-II eigensolver projects. Preprint: <https://arxiv.org/abs/1806.01036>.
- [2] P. Atkins and R. Friedman. *Molecular Quantum Mechanics, 5th Ed.* Oxford University Press, 2005.
- [3] L. S. Blackford, J. Choi, A. Cleary, E. D’Azevedo, J. Demmel, I. Dhillon, J. Dongarra, S. Hammarling, G. Henry, A. Petitet, K. Stanley, D. Walker, and R. C. Whaley. *ScaLAPACK Users’ Guide*. Society for Industrial and Applied Mathematics, 1997.
- [4] V. Blum, R. Gehrke, F. Hanke, P. Havu, V. Havu, X. Ren, K. Reuter, and M. Scheffler. *Ab initio* molecular simulations with numeric atom-centered orbitals. *Comp. Phys. Comm.*, 180:2175–2196, 2009.
- [5] C-XSC – A C++ Class Library for Extended Scientific Computing, ver. 2.5.4. <http://www.xsc.de/>.
- [6] J. Dongarra. Issue and solutions for extreme scale computing. In *HPC Asia 2018, Tokyo, Japan*, 2018.
- [7] EigenExa. <http://www.r-ccs.riken.jp/labs/lpnctr/en/projects/eigenexa/>.
- [8] EigenKernel. <https://github.com/eigenkernel/>.
- [9] ELSSES(= Extra-Large-Scale Electronic Structure calculation). <http://www.elses.jp/>.
- [10] ELPA(=Eigenvalue Solvers for Petaflop-Applications). <https://elpa.mpcdf.mpg.de/>.
- [11] FHI-AIM(= Fritz Haber Institute *ab initio* molecular simulations). <https://aimsclub.fhi-berlin.mpg.de/>.
- [12] T. Hoshi, Y. Akiyama, T. Tanaka, and T. Ohno. Ten-million-atom electronic structure calculations on the K computer with a massively parallel order- $N$  theory. *J. Phys. Soc. Jpn.*, 82:023710/1–4, 2013.
- [13] T. Hoshi, H. Imachi, K. Kumahata, M. Terai, K. Miyamoto, K. Minami, and F. Shoji. Extremely scalable algorithm for  $10^8$ -atom quantum material simulation on the full system of the k computer. *Proc. ScalA16 in SC16*, pages 33–40, 2016.
- [14] T. Hoshi, H. Imachi, A. Kuwata, K. Kakuda, T. Fujita, and H. Matsui. Numerical aspect of large-scale electronic state calculation for flexible device material. to appear in *Japan J. Indust. Appl. Math.*; Preprint: <https://arxiv.org/abs/1808.02027>.
- [15] T. Hoshi, S. Yamamoto, T. Fujiwara, T. Sogabe, and S.-L. Zhang. An order- $N$  electronic structure theory with generalized eigenvalue equations and its application to a ten-million-atom system. *J. Phys.: Condens. Matter*, pages 24/165502, 1–5, 2012.
- [16] H. Imachi and T. Hoshi. Hybrid numerical solvers for massively parallel eigenvalue computations and their benchmark with electronic structure calculations. *J. Inf. Process.*, 24:164–172, 2016.
- [17] T. Imamura, Y. Hirota, T. Fukaya, S. Yamada, and M. Machida. Eigenexa: high performance dense eigensolver, present and future. In *8th International Workshop on Parallel Matrix Algorithms and Applications (PMAA14), Lugano, Switzerland*, 2014.
- [18] D. Lee, T. Hoshi, T. Sogabe, Y. Miyatake, and S.-L. Zhang. Solution of the  $k$ -th eigenvalue problem in large-scale electronic structure calculations. *J. Comp. Phys.*, 371:618–632, 2018.
- [19] A. Marek, V. Blum, R. Johanni, V. Havu, B. Lang, T. Auckenthaler, A. Heinecke, H.J. Bungartz, and H. Lederer. The ELPA library - scalable parallel eigenvalue solutions for electronic structure theory and computational science. *J. Phys. Condens. Matter*, 26:213201, 2014.
- [20] R. M. Martin. *Electronic Structure - Basic Theory and Practical Methods*. Cambridge University Press, 2004.
- [21] ELSSES Matrix Library. <http://www.elses.jp/matrix/>.
- [22] S. Miyajima. Numerical enclosure for each eigenvalue in generalized eigenvalue problem. *J. Comput. Appl. Math.*, 236(9):2545–2552, 2012.

- [23] S. Miyajima, T. Ogita, S. M. Rump, and S. Oishi. Fast verification for all eigenpairs in symmetric positive definite generalized eigenvalue problem. *Reliable Computing*, 14:24–45, 2010.
- [24] T. Ogita and K. Aishima. Iterative refinement for symmetric eigenvalue decomposition. *Japan J. Indust. Appl. Math.*, 35(3):1007–1035, 2018.
- [25] S. M. Rump. Fast and parallel interval arithmetic. *BIT Numer. Math.*, 39(3):539–560, 1999.
- [26] S. M. Rump. INTLAB – INTerval LABoratory. In T. Csendes, editor, *Developments in Reliable Computing*, pages 77–104. Kluwer Academic Publishers, Dordrecht, 1999.
- [27] ScaLAPACK. <http://www.netlib.org/scalapack/>.
- [28] K. Tanaka, H. Imachi, T. Fukumoto, T. Fukaya, Y. Yamamoto, and T. Hoshi. EigenKernel - A middleware for parallel generalized eigenvalue solvers to attain high scalability and usability. to appear in *Japan J. Indust. Appl. Math.*; Preprint: <https://arxiv.org/abs/1806.00741>.
- [29] J. H. Wilkinson. *The Algebraic Eigenvalue Problem*. Clarendon Press, Oxford, 1965.
- [30] N. Yamamoto. A simple method for error bounds of eigenvalues of symmetric matrices. *Linear Algebra Appl.*, 324(1–3):227–234, 2001.
- [31] T. Yamamoto. Error bounds for approximate solutions of systems of equations. *Japan J. Appl. Math.*, 1(1):157–171, 1984.

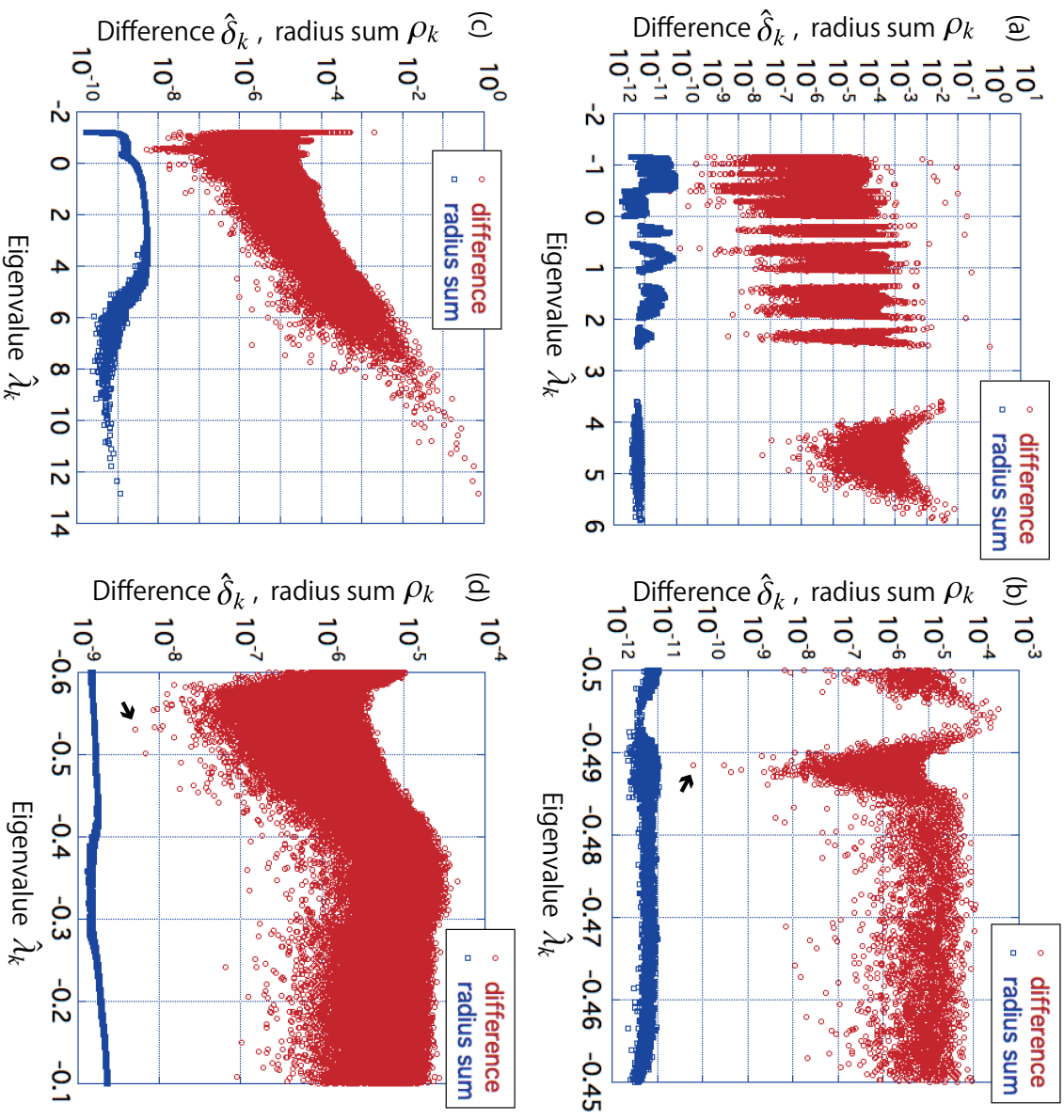


Figure 5: (a) Plot of the eigenvalue difference  $\{\hat{\delta}_k\}$  and the radius sum  $\{\rho_k\}$  as the function of the eigenvalue  $\{\hat{\lambda}_k\}$  in the case of PPE107994. (b) A close-up of (a). The arrow indicates  $\hat{\delta}_m$ . (c) Plot of the eigenvalue difference  $\{\hat{\delta}_k\}$  and the radius sum  $\{\rho_k\}$  as the function of the eigenvalue  $\{\hat{\lambda}_k\}$  in the case of NCCS430080. (d) A close-up of (c). The arrow indicates  $\hat{\delta}_m$ .